https://doi.org/10.5194/egusphere-2023-3009
Preprint. Discussion started: 21 December 2023
© Author(s) 2023. CC BY 4.0 License.

Dissolved Nitric Oxide in the Lower Elbe Estuary and the Hamburg Port Area

Riel Carlo O. Ingeniero[1], Gesa Schulz[2,3], Hermann W. Bange[1]

[1]Marine Biogeochemistry Research Division, GEOMAR Helmholtz Centre for Ocean Research Kiel, Düsternbrooker Weg 20, Kiel, 24105 Germany
[2] Institute of Geology, Center for Earth System Research and Sustainability (CEN), Universität Hamburg, Hamburg, 20146, Germany
[3]Institute of Carbon Cycles, Helmholtz-Zentrum Hereon, Geesthacht, 21502, Germany

Correspondence to: Riel Carlo O. Ingeniero (ringeniero@geomar.de)

Abstract. Nitric oxide (NO) is an intermediate of various microbial nitrogen cycle processes and the open ocean and coastal areas are generally a source of NO in the atmosphere. However, our knowledge about its distribution and the main production processes in coastal areas and estuaries is rudimentary at best. To this end, dissolved NO concentrations were measured for the first time in surface waters along the lower Elbe Estuary and Hamburg Port area in July 2021. The discrete surface water samples were analyzed using a chemiluminescence detection method. The NO concentrations ranged from below the limit of detection (9.1×10^{-12} mol L^{-1}) to 17.7×10^{-12} mol L^{-1}, averaging at 12.5×10^{-12} mol L^{-1} and were supersaturated in the surface layer of both the lower Elbe Estuary and the Hamburg Port area, indicating that the study site was a source of NO to the atmosphere during the study period. On the basis of a comprehensive comparison of NO concentrations with parallel nutrient, oxygen, and nitrous oxide concentration measurements, we conclude that the observed distribution of dissolved NO was most likely resulting from microbial nitrogen transformation processes, particularly nitrification in the coastal-brackish and limnic zones of the lower Elbe Estuary and nitrifier-denitrification in the Hamburg Port area.

1 Introduction

Nitric oxide (NO) is an atmospheric trace gas that is rapidly oxidized to atmospheric nitrogen dioxide (NO_2). NO_x (= NO + NO_2) is a significant contributor to photochemical smog (Haagen-Smit and Fox, 1954), a cause of acid rain (Likens et al., 1979; Fanning, 1989), and affecting tropospheric ozone (O_3) (Haagen-Smit and Fox, 1954). Atmospheric NO_x has an atmospheric lifetime ranging from hours to days (IPCC, 2021). Because of its atmospheric reactions yielding O_3, methane, and nitrate aerosols, it is an indirect greenhouse gas with an overall negative efficient radiative forcing (IPCC, 2021).

The major sources of atmospheric NO_x are emissions from fossil fuel combustion and soils (Jaeglé et al., 2005). However, little is known about the distribution as well as the production and consumption processes of NO in the marine environment. Zafiriou et al. (1980) measured the dissolved NO concentration in seawater for the first time in the central equatorial Pacific Ocean. They noted that the ocean could be a source of NO to the atmosphere due to its photochemical production from dissolved nitrite (NO_2^-). NO is also an important intermediate of microbial nitrogen cycle processes such as denitrification,

https://doi.org/10.5194/egusphere-2023-3009
Preprint. Discussion started: 21 December 2023
© Author(s) 2023. CC BY 4.0 License.

nitrification, and anammox (Schreiber et al., 2012; Kuypers et al., 2018). Moreover, NO was identified as a signal molecule on a cellular level in many marine organisms and between bacteria and algae (see Abada et al., 2023).

The determination of dissolved NO concentration is challenging because of its reactivity, which results in a very short lifetime in (sea)water (Lancaster, 1997). Nevertheless, measurements of dissolved NO in aquatic environments such as open and coastal oceans and rivers have received increasing attention during the last decade. Examples of recent NO measurement campaigns include those in the Kurose River in Japan (Anifowose et al., 2015), the Seto Inland Sea in Japan (Olasehinde et al., 2010), the tropical Northwestern Pacific Ocean (Tian et al., 2019), the oxygen minimum zone off the coast of Peru (Lutterbeck and Bange, 2015; Lutterbeck et al., 2018), and the coastal seas off Qingdao (Tian et al., 2021).

This paper presents the first measurement of dissolved NO concentrations in the lower Elbe Estuary and Hamburg Port basins during a ship campaign in July 2021. The overarching objectives of our study were (i) to determine the distribution of dissolved NO along the salinity gradient, (ii) to estimate the flux density of NO across the water/atmosphere interface, and (iii) to identify the potential production pathways and controlling factors on NO distribution in the lower Elbe Estuary and Hamburg Port area.

2 Methods

2.1 Study site

Originating from the Karkonosze Mountains in the northern region of the Czech Republic, the Elbe River basin is the fourth largest catchment area (148,268 km^2) in Central Europe (Amann et al., 2012) with average long-term freshwater runoff of about 720 $m^3 s^{-1}$ (Kerner, 2007). Its estuarine part stretches about 140 km from the weir in Geesthacht to the coastal city of Cuxhaven in Lower Saxony, Germany.

The Elbe Estuary is considered the most significant riverine nitrogen source in the German Bight of the North Sea (Dähnke et al., 2008). It is a turbid and well-mixed estuarine system with a maximum turbidity zone near Brunsbüttel at Elbe-km 698 (Burchard et al., 2017; Kappenberg and Grabemann, 2001). It has semi-diurnal tidal ranges of 2 to 4 meters, and its wind conditions are dominated by westerly winds (Hein et al., 2021). Generally, the Elbe Estuary is deepened and dredged to maintain a water depth of 15 to 20 m to grant access for large container ships into the Port of Hamburg (Kerner, 2007).

Its water residence time is estimated to range between 3 to 22 days (Geerts et al., 2012), with longer residence times during summer when the river discharge is low (Hein et al., 2014). The dissolved NO concentration in the surface water of the Elbe Estuary was measured at various sampling points from the mouth of the estuary to the Hamburg Port area, as shown in Fig. 1. Sampling was performed upstream against the outgoing tide to prevent tidal effects on our measurements.

https://doi.org/10.5194/egusphere-2023-3009
Preprint. Discussion started: 21 December 2023
© Author(s) 2023. CC BY 4.0 License.

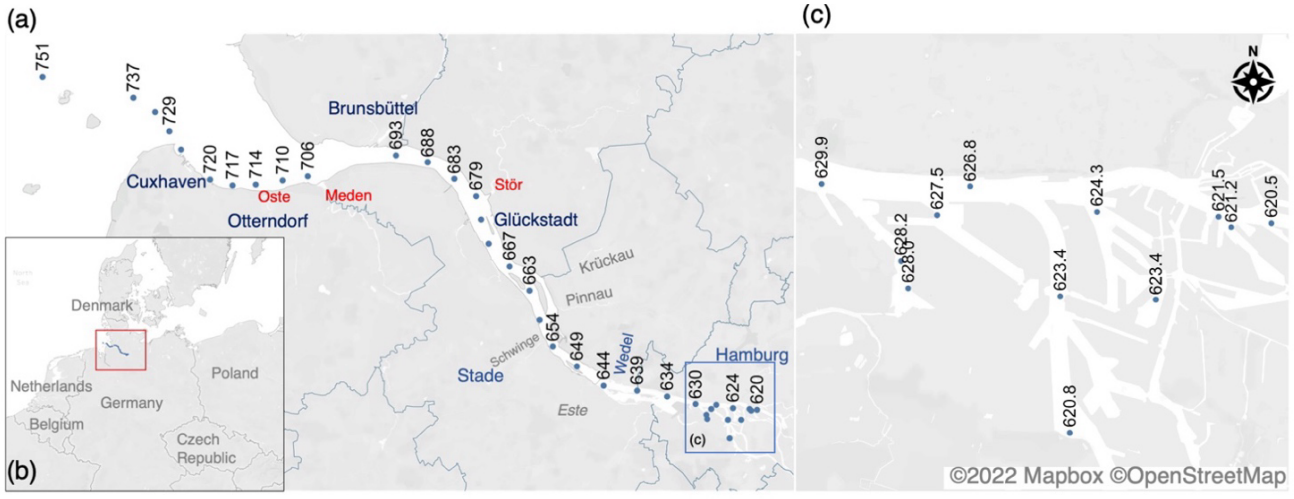

Figure 1: a) Map of the sampling locations with corresponding stream kilometers and b) the relative position of the sampling area in Northern Europe. c) A higher-resolution map of the sampling points in the Hamburg Port area from Elbe-km 620 to 630. The given Elbe-km in this study refers to the distance from the point where the Elbe passes the border from the Czech Republic to Germany. Note that in this study, we used the following salinity zoning: the brackish-coastal zone downstream of Elbe-km 690, the limnic zone from Elbe-km 630 to 690, and the Hamburg Port area (or Port) located from Elbe-km 620 to 630. Background map: ©OpenStreetMap 2022. Distributed under the Open Data Commons Open Database License (ODbL) v1.0.2.

2.2 Sampling

Surface water was sampled on board the RV *Ludwig Prandtl* during a campaign from 27 to 29 July 2021, using a FerryBox flow-through system (Petersen et al., 2014). The system draws water from approximately 1.2 m below the water surface through a membrane pump. The FerryBox continuously measures in situ biogeochemical parameters such as dissolved oxygen (O_2), pH, salinity, and water temperature. The sensors in the FerryBox system were routinely calibrated or compared to established standard methods beforehand. For instance, the optode measurements were compared with the Winkler titration method, leading to an oxygen correction of $1.12 \times [O_{2,corr}] + 13.41$ ($R^2 = 0.97$), and the salinity measurements with the Optimare Precision Salinometer (Bremerhaven, Germany).

Discrete water samples were collected for analysis of nutrients, chlorophyll a, and dissolved NO every 20 minutes from the Ferrybox system bypass using field sampling collection, preservation, and storage methods described in detail in earlier related publications (Schulz et al., 2022; Norbisrath et al., 2022).

Nitrous oxide (N_2O) concentrations were measured continuously from a bypass of the FerryBox system using laser-based off-axis integrated cavity output (OA_ICOS) absorption spectroscopy (Model 914-0022, Los Gatos Res. Inc., San Jose, CA, USA) coupled with a (sea)water/gas equilibrator. The details of the N_2O measurements are described in Schulz et al. (2023). Furthermore, wind speeds at 10 m height were measured onboard with a MaxiMet GMX600 (Gill Instruments, Ltd., Saltash, UK) weather station.

https://doi.org/10.5194/egusphere-2023-3009
Preprint. Discussion started: 21 December 2023
© Author(s) 2023. CC BY 4.0 License.

2.3 Measurement of dissolved NO

Because of the short lifetime of NO, triplicate NO samples were measured within 20 minutes after sampling following the method described by Lutterbeck and Bange (2015). During this campaign, we used a portable calibrator (2BTech Model 714 NO2/NO/O3 Calibration Source™) to calibrate the NO detector (Birks et al., 2020). The resulting gas output from the calibrator covered the detection range of the NO detector from 0 to 1000 ppb NO. A schematic diagram of the minor update to the components in the analytical method described in Lutterbeck and Bange (2015) is shown in Fig. S1.

NO signal outputs by the NO detector were recorded using PuTTY 0.78, a free and open-source client application for Windows. To determine NO mole fractions, the Rieman integrals of the signal peaks were calculated using the MATLAB (2022b) trapezoidal numerical integration function trapz. After applying a linear calibration curve of aqueous NO standard solutions prepared according to Lutterbeck and Bange (2015), the final concentrations of dissolved NO (C_w in mol L^{-1}) were computed with Eq. (1):

$$C_w = x'_{sw} \times P \times K_H \quad (1)$$

where x' is the measured mole fraction of NO from the water sample, P is the atmospheric pressure, and K_H is the Henry's law constant for NO (1.9×10^{-3} mol L^{-1} atm^{-1}) (see Zacharia and Deen, 2005).

The instrument limit of detection (LOD) was computed as 3 times the standard deviation (σ) of the blank or zero calibration point. During this campaign, the instrument limit of detection was 9.1 pM, while the average relative standard error was approximately ± 26 %. NO concentrations < LOD were omitted in further calculations.

2.4 Estimation of NO flux density and saturation ratios.

The flux of NO at the water–air boundary (F_{NO}, in mol cm^{-2} s^{-1}) was estimated using Eq. (2) from Anifowose and Sakugawa (2017):

$$F_{NO} = k_w \times (C_w - K_H\, p_{NO}) \times 10^{-1} \quad (2)$$

where k_w is the liquid phase transfer velocity (m s^{-1}), and p_{NO} is the partial NO (atm) pressure in the overlying atmosphere. The value of k_w expressed in m s^{-1} was determined according to Borges et al. (2004) (see also Brase et al., 2017):

$$k_w = (360000)^{-1} \times (4.045 + 2.58\, U) \times \left(\frac{S_c}{600}\right)^{-0.5} \quad (3)$$

$$S_c = \frac{\nu_{sw}}{D} \quad (4)$$

where U is the wind speed at 10 m height (m s^{-1}), S_c is the Schmidt number, ν_{sw} is the kinematic viscosity of surface water, and D is the diffusion coefficient of NO in water. U measured onboard ranged from 1.76 to 8.86 m s^{-1}, with a mean ± standard deviation (SD) wind speed at the sampling stations of 5.78 ± 2.12 m s^{-1}. The kinematic viscosity (ν_{sw}, in m^2 s^{-1}) was calculated using the following equation:

$$\nu_{sw} = \frac{\mu_{sw}}{\rho} \quad (5)$$

https://doi.org/10.5194/egusphere-2023-3009
Preprint. Discussion started: 21 December 2023
© Author(s) 2023. CC BY 4.0 License.

where the dynamic viscosity of surface water (μ_{sw}, in kg m^{-1} s^{-1}), a function of temperature (T) and salinity (S), was estimated using Eqs. (6 –9) from Sharqawy et al. (2010), while density (ρ, in kg m^{-3}) was determined using a MATLAB (2022b) function from Ruiz-Martinez (2021) derived from Gill (1983).

$$\mu_{sw} = \mu_w (1 + AS + BS^2) \quad (6)$$

$$A = 1.541 + (1.998\, x\, 10^{-2}\, T) - (9.52\, x\, 10^{-5}\, T^2) \quad (7)$$

$$B = 7.974 - (7.561\, x\, 10^{-2}\, T) + (4.724\, x\, 10^{-4}\, T^2) \quad (8)$$

$$\mu_w = 4.2844 \times 10^{-5} + (0.157\,(T + 64.993)^2 - 91.296)^{-1} \quad (9)$$

The NO diffusion coefficient (D, × 10^{-9} m^2 s^{-1}) was calculated according to Wise and Houghton (1968):

$$D = 0.9419\, exp\,(0.0447\, T) \quad (10)$$

Furthermore, the NO saturation ratio (NO_{sat}) was calculated based on the measured NO concentration in surface water (NO_{sw}) and in the NO concentration (NO_{eq}) in equilibrium with the mole fraction of NO (x'_{NO}) in the overlying atmosphere :

$$NO_{sat}\,\% = 100 \times \frac{C_w}{C_{eq}} \quad (11)$$

$$C_{eq} = p_{NO} \times K_H = x'_{NO} \times P \times K_H \quad (12)$$

where P is the total ambient pressure set to 1 atm. In this study, it is important to note that the flux density is a rough approximation since the atmospheric NO mole fraction (x'_{NO}) was not measured on board but estimated from the air monitoring data available from https://luft.hamburg.de/ (last accessed on 2 May 2023). The mean hourly atmospheric NO concentrations (mole fractions) measured at seven air monitoring stations in the Hamburg Port area during the study period (see Fig. S2) ranged from 2.00 µg m^{-3} (1.60 ppb) to 8.25 µg m^{-3} (6.60 ppb), with a mean ± SD concentration of 4.30 ± 1.76 µg m^{-3} (3.4 ± 1.41 ppb). The mean atmospheric NO mole fraction of 3.4 ± 1.41 ppb was used to estimate C_{eq} with Henry's law constant (Eq. 12).

2.5 Measurement of ancillary biogeochemical parameters

Dissolved inorganic nitrogen concentrations (nitrate (NO_3^-), nitrite (NO_2^-), and ammonium (NH_4^+)) were measured spectrophotometrically (Dafner, 2015) using air-segmented flow analysis techniques (SEAL AutoAnalyzer 3, SEAL Analytical, Germany). The total dissolved inorganic nitrogen (DIN) was calculated from the sum of NO_3^-, NO_2^-, and NH_4^+ concentrations. The limits of detection were as follows: 0.05 µmol L^{-1} for NO_3^-, 0.05 µmol L^{-1} for NO_2^-, and 0.07 µmol L^{-1} for NH_4^+.

Chlorophyll a was extracted in 90% acetone overnight, measured photometrically (Hach Lange DR-6000), and calculated using the parametrization by Jeffrey and Humphrey (1975).

2.6 Data analysis

Calculations for apparent oxygen utilization (AOU), N_2O saturation, N_2O sea(water)-to-air flux density, and excess N_2O (ΔN_2O) are discussed in Schulz et al. (2023). The data in this study were visualized using Origin 10.5.117 and MATLAB

https://doi.org/10.5194/egusphere-2023-3009
Preprint. Discussion started: 21 December 2023
© Author(s) 2023. CC BY 4.0 License.

(2022b). Statistical analyses, including mean, median, standard deviation (SD), and Pearson's correlation (R), were performed with MATLAB (2022b). Results with p-values < 0.05 were considered statistically significant at a 95 % confidence level.

3. Results

3.1 Biogeochemical setting along the estuary

Figure 2 presents a scatter plot of various near-surface biogeochemical parameters measured from the North Sea to the Hamburg Port area during the campaign (see also Figure S3). As seen in Fig. 2, we can generally observe the mixing of warmer, less oxygenated, more acidic, and nutrient-rich waters of the Elbe Estuary with North Sea waters.

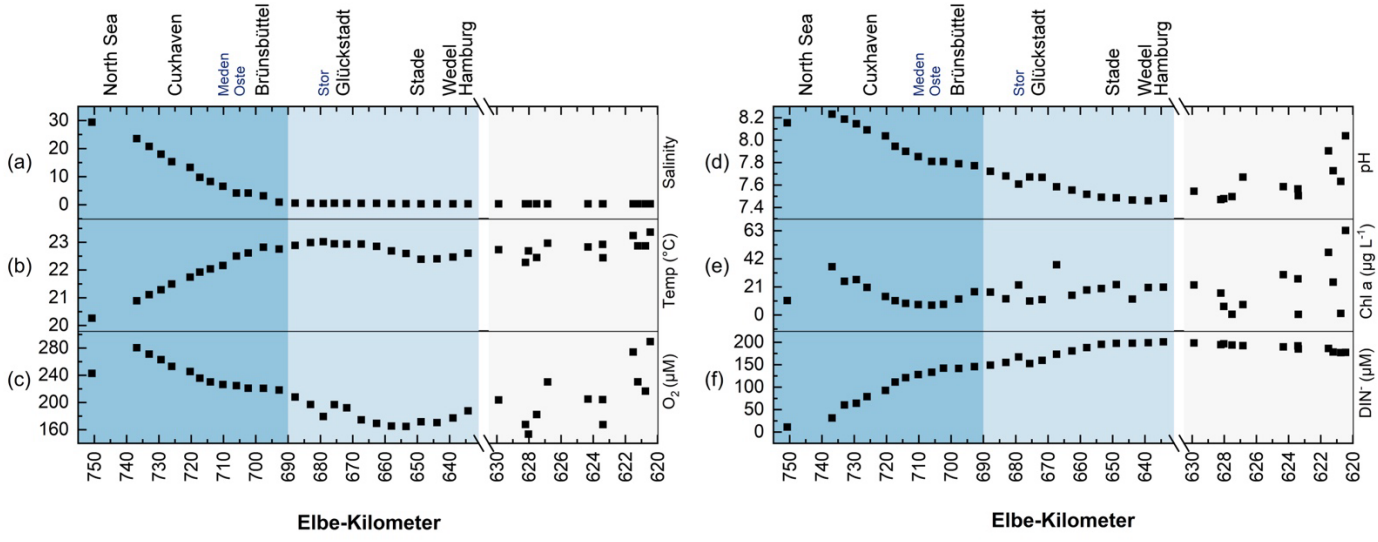

Figure 2: Distribution of various surface biogeochemical parameters along the Elbe Estuary from the North Sea to Hamburg Port area– (a) salinity, (b) temperature (°C), (c) oxygen concentration (µM), (d) pH, (e) chlorophyll a concentration (µg L^{-1}), and (f) dissolved inorganic nitrogen (µM). Note that we divided the graph into three distinct salinity zones: the brackish-coastal zone downstream of Elbe-km 690, the limnic zone from Elbe-km 630 to 690, and the Hamburg Port area located from Elbe-km 620 to 630. The zones can be distinguished through a contrast of blue, indicating a decrease in salinity.

Surface salinity (Fig. 2a) ranged from 0.31 (Hamburg Port area) to 29.43 (North Sea, Elbe-km 751). A pronounced salinity difference of 6.0 was observed between the North Sea's surface waters (Elbe-km 751) and the estuary's mouth near Cuxhaven (Elbe-km 737). From Elbe-km 737, salinity decreased linearly (0.54 km^{-1}, $p=2.97 \times 10^{-6}$) until Elbe-km 693 (near Brunsbüttel). From Elbe-km 693, salinity gradually declined to about 0.31, approaching the Hamburg Port area. Based on these salinity values, we divided the study site into three distinct zones: the brackish-coastal zone downstream of Elbe-km 690, the limnic zone from Elbe-km 630 to Elbe-km 690, and the Hamburg Port area from Elbe-km 620 to 630.

https://doi.org/10.5194/egusphere-2023-3009
Preprint. Discussion started: 21 December 2023
© Author(s) 2023. CC BY 4.0 License.

The surface temperature (Fig. 2b) steadily increased upstream due to the warmer outflow water from the Elbe River in summer. From 20.26 °C in the North Sea (Elbe-km 751), the temperature increased to 23.03 °C near Glückstadt (Elbe-km 679). Upstream of Elbe-km 679, the water temperature ranged from 22.27 °C to 23.37 °C, with the highest surface water temperature of 23.37 °C recorded in the Hamburg Port area at Elbe-km-620.46. This site also had the highest chlorophyll a and oxygen concentrations of 63.3 µg L^{-1} and 289.6 µM (saturation: 109.2 %), respectively.

The O_2 concentration (Fig. 3b) in the North Sea was 242.8 µM (102.3 % saturation) and thus slightly lower than the O_2 concentration of 280.6 µM (115.6 % saturation) at Elbe-km 737. Upstream of Elbe-km 737, the O_2 concentration decreased to 179.5 µM (67.3 % saturation) near Glückstadt. From Glückstadt to near Wedel, the O_2 concentration generally declined, ranging from 170.5 µM (63.1 % saturation) to 179.5 µM (67.3 % saturation). In the Hamburg Port area, the O_2 concentration is highly dynamic, ranging from 153.5 µM (57.1 % saturation) to 289.6 µM (109.2 % saturation), following the pH and chlorophyll a concentration trend. The minimum O_2 concentrations in the campaign were also measured in this location, near Elbe-km 628 and Elbe-km 623.

The trend in pH (Fig. 2d) was analogous to the trend in oxygen concentrations. At Elbe-km 751 in the North Sea, the measured pH value was 8.15, which is also slightly lower than that at Elbe-km 737 (pH 8.23). From Elbe-km 737, the pH decreased to the lowest measured pH during the entire field campaign (pH 7.46) near Wedel.

Furthermore, the chlorophyll a concentrations ranged from 0.46 µg L^{-1} to 46.9 µg L^{-1} (Fig. 2e). Notably, the minimum and maximum chlorophyll a concentrations were measured in the Hamburg Port area at Elbe km 623 and 622, respectively. No distinguishable spatial pattern on chlorophyll a concentration was observed, except that a distinct peak in chlorophyll a concentration coincided with the maximum suspended particulate matter (SPM) concentration (not shown) of 412.5 mg L^{-1} at Elbe-km 667.4 near Glückstadt.

Overall, the DIN concentrations (Fig. 2f) increased from the mouth of the estuary upstream, with the highest concentrations recorded in the Hamburg Port area (see also Fig. S3). Further details on the concentration of the DIN substrates are presented in the next section.

In the supplementary material, we provided a table presenting the summary statistics (Table S1) and box plots (Figure S3) of the biogeochemical parameters measured in this study.

3.2 Distribution of N_2O and dissolved inorganic nitrogen (DIN) concentrations

Figure 3 shows the distribution of N_2O and DIN components in the study area, while Fig. 4 presents box plots of the data in each salinity zone. The N_2O concentrations (Fig. 3a) ranged from 9.1 nM (Elbe-km 737) to 38.0 nM (Elbe-km 628.04), with a mean ± SD concentration of 18.0 ± 6.5 nM and a median concentration of 16.6 nM (see also Schulz et al., 2023).

https://doi.org/10.5194/egusphere-2023-3009
Preprint. Discussion started: 21 December 2023
© Author(s) 2023. CC BY 4.0 License.

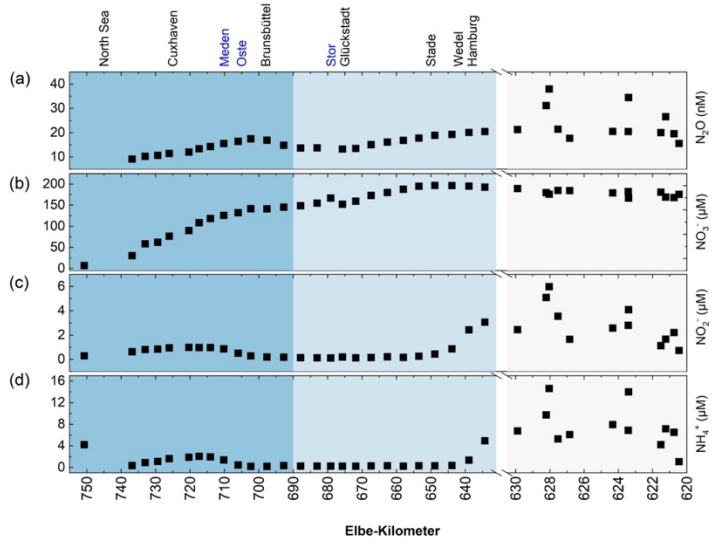

Figure 3: Scatter plot of concentrations of (a) N_2O, (b) NO_3^-, (c) NO_2^-, and (d) NH_4^+ along the Elbe Estuary.

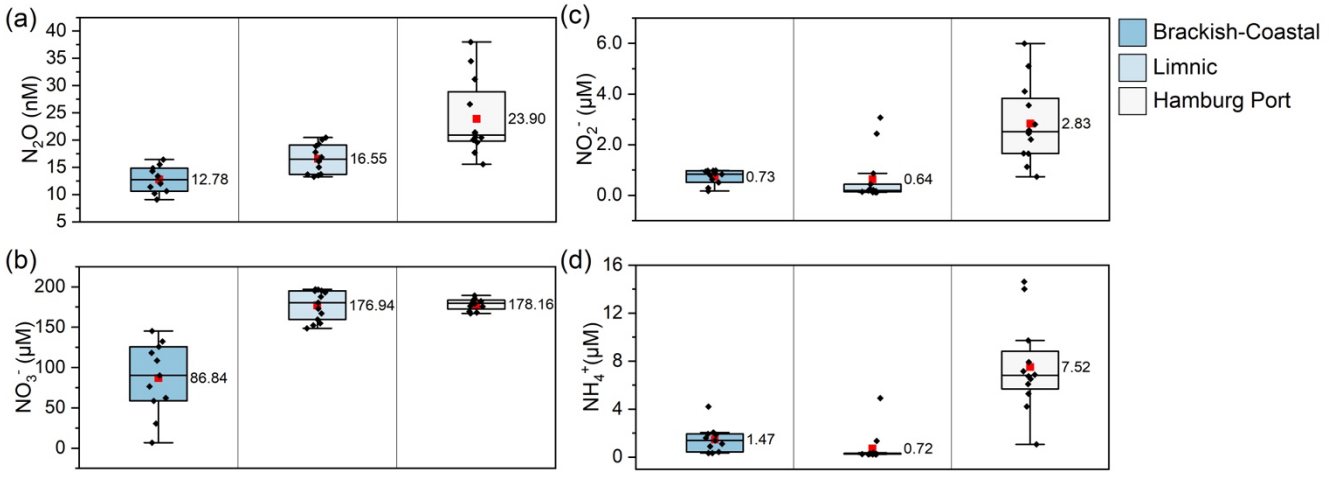

Figure 4: Box plot of concentration of (a) N_2O, (b) NO_3^-, (c) NO_2^-, and (d) NH_4^+ in each salinity zone along the Elbe Estuary. The boxes represent the interquartile range (IQR), with the lower and upper whiskers extending to the 25th and 75th percentiles, respectively. The median line is shown in the center of each box, and the mean is represented by a red square.

Enhanced N_2O concentrations (mean: 23.9 ± 7.1 nM) were measured in the Hamburg Port area (Fig. 3a). Notable higher N_2O concentrations were observed in the Hamburg Port area at Elbe-km 628.04, 628.21, and 623.40 (Fig. 2a). At these locations, dissolved N_2O concentrations exceeded 30 nM. The N_2O were supersaturated at 440 %, 361 %, and 401 %, respectively, with corresponding fluxes of 131, 116, and 133 µM m^{-2} d^{-1} (data are taken from Schulz et al., 2023).

https://doi.org/10.5194/egusphere-2023-3009
Preprint. Discussion started: 21 December 2023
© Author(s) 2023. CC BY 4.0 License.

The DIN (Fig. 2f) generally increased from the mouth of the estuary upstream until it reached around 200 µM in the Hamburg Port area. The trend was driven by its primary component, NO_3^-, which reached its maximum of 196.89 µM in the limnic zone at Elbe-km 649 before entering the Hamburg Port area (Fig. 3b). Upstream of this point, the NO_3^- concentrations were lower. NO_2^- and NH_4^+ concentrations closely followed similar trends (Figs. 3c and 3d), with slightly higher mean concentrations in the brackish–coastal zone than in the limnic zone (Figs. 4c and 4d). An increase in NO_2^- and NH_4^+ concentrations was also observed downstream of the maximum turbidity zone (Dähnke et al., 2022) at the confluence of River Oste and Meden. NO_2^- and NH_4^+ concentrations increased from Elbe-km 650 to the Hamburg Port area, where significant variability in their concentrations was observed. The spikes in NO_2^- and NH_4^+ concentration coincided with those in N_2O concentration at the Hamburg Port basins at Elbe-km 623.40, 628.04, and 628.21.

3.3 Dissolved NO concentrations, saturation ratios, and flux densities

NO concentrations in surface water of the Elbe Estuary (from Elbe-km 737 to Elbe-km 620, n=35) ranged from < LOD to 17.7 pM, with a mean ± SD concentration of 12.5 ± 1.9 pM and a median concentration of 12.1 pM (Fig 5a). Near the mouth of the estuary, the NO concentrations of five samples were below the detection limit. Concentrations started to increase slightly above the detection limit at the outflow of the River Meden near Otterndorf at Elbe-km 710 and 714. The measured NO concentration remained steady at around 12.0–13.0 pM in the limnic zone of the estuary, with a slightly enhanced concentration at Elbe-km 676 (13.7 pM), a sampling site in the port of Glückstadt.

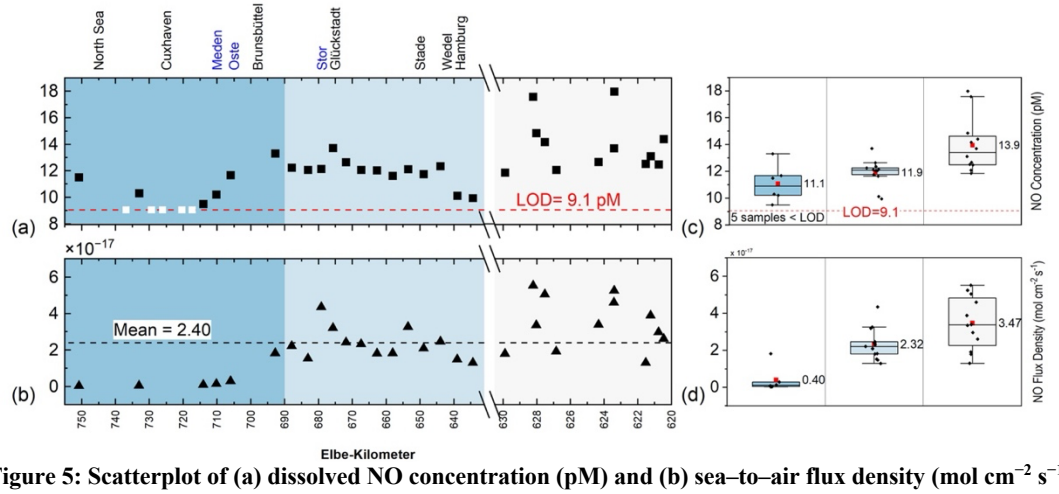

Figure 5: Scatterplot of (a) dissolved NO concentration (pM) and (b) sea–to–air flux density (mol cm^{-2} s^{-1}) estimates along the Elbe Estuary. Boxplot of (c) dissolved NO concentration and (d) sea–to–air flux density estimates along the Elbe Estuary. Note that the mean atmospheric NO concentration of 4.30 µg m^{-3} at seven background air monitoring stations in Hamburg located proximate to the Elbe Estuary was used to estimate the flux density.

Further upstream, high NO concentrations in the Hamburg Port area were observed, with peaks of 17.7 pM at Elbe-km 623.40 and 17.6 pM at Elbe-km 628.21. Generally, average NO concentrations increased as salinity decreased (Fig. 5c), with a mean

https://doi.org/10.5194/egusphere-2023-3009
Preprint. Discussion started: 21 December 2023
© Author(s) 2023. CC BY 4.0 License.

± SD concentration of 11.1 ± 1.4 pM in the brackish-coastal zone, 11.9 ± 1.1 pM in the limnic zone, and 13.9 ± 2.0 pM in the Hamburg Port area.

The NO saturation values (excluding < LOD) ranged from 147 to 274 %, with mean saturation values of 172 %, 184 %, and 216 % in the brackish-coastal zone, limnic zone, and the Hamburg Port area, respectively. The overall mean ±SD and median NO saturations in the surface layer of the Elbe Estuary were 194 ± 29 % and 189 %, respectively.

Moreover, the NO flux density (excluding < LOD) ranged from 3.1×10^{-19} to 5.5×10^{-17} mol cm^{-2} s^{-1}, with overall mean ± SD and median flux densities of 2.4 (±1.5) $\times 10^{-17}$ mol cm^{-2} s^{-1} and 1.58×10^{-17} mol cm^{-2} s^{-1}, respectively (Figure 5b). The mean NO flux densities also generally increased as salinity decreased (Fig. 5d).

4. Discussion

4.1 NO concentrations and flux densities

Figure 6 shows a compilation of average dissolved NO concentrations and estimated flux densities from previous studies. The mean NO concentration of 12.5 ± 1.9 pM from our study is at the lower end of the range of previously published measurements from the marine environment.

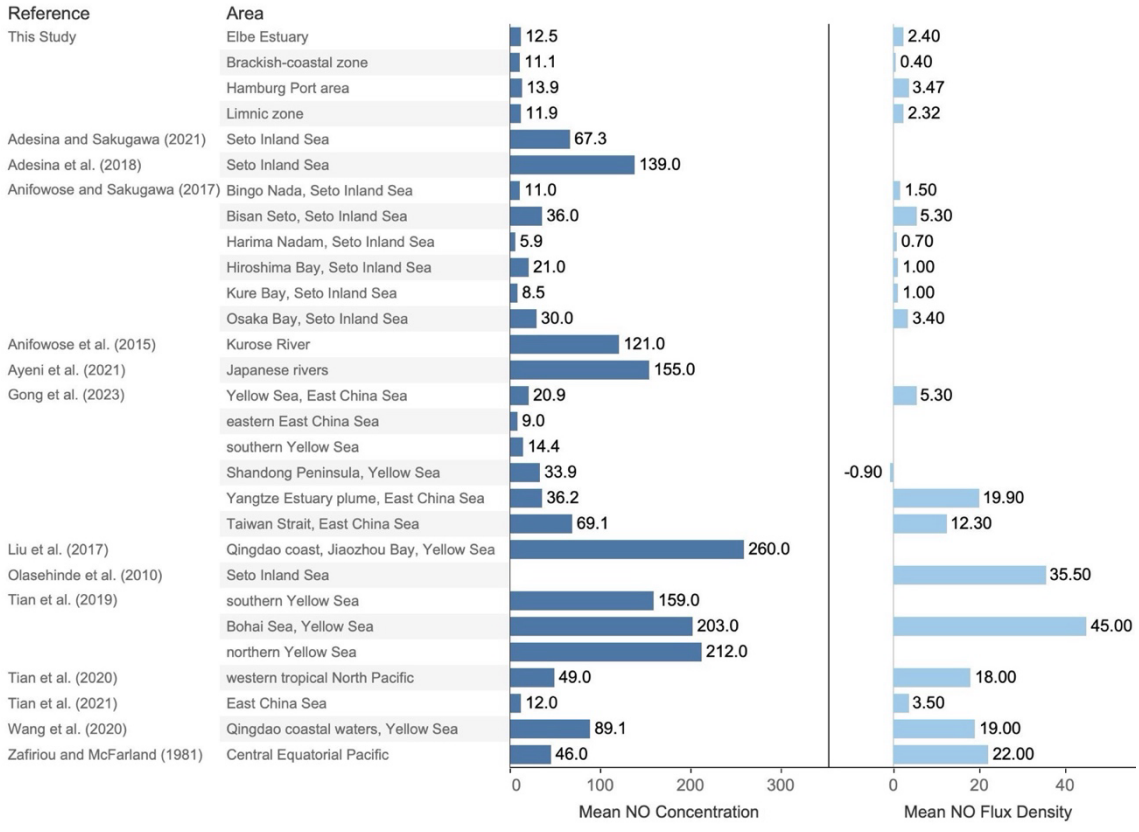

Figure 6: Comparison of the mean dissolved NO concentration (pM) and estimated sea–to–air flux density (× 10^{-17} mol cm^{-2} s^{-1}) from previous studies and the present study.

https://doi.org/10.5194/egusphere-2023-3009
Preprint. Discussion started: 21 December 2023
© Author(s) 2023. CC BY 4.0 License.

As mentioned in Sect. 3.5, NO was supersaturated in the surface layer of the Elbe Estuary, indicating that the Elbe Estuary, particularly the Hamburg Port area, was a source of NO to the atmosphere during the study period. The mean estimated flux density in this study is close to the average flux density from the Kurose River reported by Anifowose and Sakugawa (2017) but at the lower end of flux densities reported from shelf and open ocean waters.

The observed variations in NO concentrations and flux densities along the salinity gradient indicate potential changes in NO production pathways and controlling factors that influence NO distribution in the entire Elbe Estuary and at each salinity zone, which we discuss in the following sections. The correlation analysis between NO and various biogeochemical parameters is presented in Table S3.

4.2 Salinity and freshwater input influencing NO concentrations

Along the salinity gradient, the average NO concentrations tend to increase from the North Sea towards the Elbe River (Sect. 3.3). Although this negative correlation is not statistically significant (Table S3), the negative slope suggests a potential inverse relationship, in which a decrease in salinity appears to coincide with an increase in NO concentration, which could potentially be attributed to DIN input from the Elbe River. This finding has been observed in prior studies by Gong et al. (2023), Adesina et al. (2021), and Tian et al. (2019), which have identified a similar negative trend between dissolved NO concentrations and salinity.

Specifically, Gong et al. (2023) found that salinity had a significant negative correlation with dissolved NO concentration ($r = -0.44$, $p < 0.05$, $n = 13326$), while Adesina et al. (2021) reported an even stronger correlation for steady-state NO concentration versus salinity ($r = -0.83$, $p < 0.01$). Furthermore, Adesina et al. (2018) reported a negative correlation between salinity and NO photochemical generation rate ($r = -0.504$, $p > 0.05$). Meanwhile, Tian et al. (2019) observed an inverse relationship between salinity and surface dissolved NO concentrations for stations affected by the outflow of the Yellow River in the southern Bohai Sea and ascribed it to high DIN input.

In the Kurose River, Ayeni et al. (2021) examined the spatial variability of NO concentrations and identified a gradient from low concentrations in the upstream sections to higher concentrations in the downstream sections, the latter being notably influenced by anthropogenic activities. Moreover, Gong et al. (2023) discussed that NO distribution is likely influenced by freshwater inputs due to the ready availability of precursor DIN substrates. Nonetheless, similar to what we observed, Gong et al. (2023) noted that salinity is insufficient to explain the uneven distribution of NO at their study site, indicating that other parameters influence NO concentrations along the Elbe Estuary.

4.3 Dissolved inorganic nitrogen influencing NO concentrations

There are two widely known sources of NO in surface seawater: NO_2^- photolysis and biological production. It is well reported that NO_2^- is the primary source of NO in seawater through photolysis (Treinin and Hayon, 1970; Zafiriou et al., 1980; Anifowose et al., 2015) as shown in R1 below:

$$NO_2^- + H_2O + h\nu \rightarrow NO + OH + NO^- \; where \; h\nu = 295 \leq \lambda \leq 410 \text{ nm} \quad \text{(R1)}$$

https://doi.org/10.5194/egusphere-2023-3009
Preprint. Discussion started: 21 December 2023
© Author(s) 2023. CC BY 4.0 License.

However, the mechanism of how nitrogen-containing nutrients (NO_3^-, NO_2^-, NH_4^+) and their cycling affect the dissolved NO distribution in aquatic environments remains unresolved. In this study, the NO_3^-, NO_2^-, and NH_4^+ concentrations were higher than those found in previous studies in the river and coastal areas (e.g., Ayeni et al., 2021; Gong et al., 2023; Liu et al., 2017); however, the elevated concentrations did not correspond to a higher average dissolved NO concentration in the Elbe Estuary. Some studies (e.g., Olasehinde et al., 2010; Anifowose et al., 2015; Anifowose and Sakugawa, 2017; Ayeni et al., 2021; Gong et al., 2023) observed positive correlations between NO concentrations or photoproduction rates and NO_2^- concentrations. In contrast, other studies (Tian et al., 2020, 2021) did not observe any relationship between surface NO distribution and concentrations of NO_3^-, NO_2^-, and NH_4^+.

Gong et al. (2023) argued that nitrogen-containing nutrients may serve as the substrate or intermediate for photochemical and microbial NO production; thus, high concentrations of NO_3^-, NO_2^-, and NH_4^+ ensure that the necessary conditions for NO production are met. Nevertheless, they also noted areas in their study site (i.e., the nearshore region of the Shandong Peninsula) where the DIN concentrations were significantly lower yet had high surface dissolved NO concentration, attributing it to the uptake of atmospheric NO into the surface layer. Likewise, Ayeni et al. (2021) also noted that some rivers in Japan with higher NO_2^- concentrations had lower rates of photoproduction of NO and vice versa, attributing these imbalances to nitrogen cycling processes (nitrification, denitrification, and anammox), which could produce or consume NO, or the photochemical transformation of organic nitrogen from dissolved organic matter producing NO_2^- to form NO in areas with low NO_2^-.

Shown in Table 1 is a correlation analysis between NO and the DIN substrates. Using the entire data set (i.e., "Overall"), we observed a significant positive correlation between NO and NO_2^-, NH_4^+, the sum of NO_2^- and NH_4^+, N_2O, and NO_2^-/O_2 ratio. Drawing solely from these findings, one might infer that elevated concentrations of NO_2^- and NH_4^+ invariably lead to an increase in NO concentration.

Table 1: Pearson correlation coefficient (R) between NO and some nitrogen parameters at each salinity zone. Significant correlations are denoted in bold font. Note that the superscripts after the R values indicate a significant correlation at $^a p < 0.001$, $^b p < 0.01$, and $^c p < 0.05$.

	Overall	Coastal-Brackish	Limnic	Hamburg Port
DIN (µM)	0.3264	0.1630	**–0.6576^c**	0.0677
NO_3^- (µM)	0.2552	0.1715	**–0.5998^c**	–0.3726
NO_2^- (µM)	**0.5425^b**	**–0.9419^b**	**–0.8380^a**	**0.6570^c**
NH_4^+ (µM)	**0.6051^a**	–0.2267	**–0.7323^b**	0.5558
$NO_2^- + NH_4^+$ (µM)	**0.6005^a**	–0.4396	**–0.8011^a**	**0.6060^c**
NO_2^-/O_2 ratio	**0.5692^a**	**–0.9212^b**	**–0.8404^a**	**0.6711^c**
N_2O (nM)	**0.6609^a**	0.3164	**–0.7527^b**	**0.6940^c**
N_2O/ NO_2^- ratio	–0.1196	**0.9422^c**	**0.6064^c**	–0.2644
N_2O/ NH_4^+ ratio	–0.1833	**0.9589^b**	**0.7569^b**	0.0195
$N_2O/(NO_2^- + NH_4^+)$ ratio	–0.1550	**0.9881^b**	**0.7014^c**	–0.0409

https://doi.org/10.5194/egusphere-2023-3009
Preprint. Discussion started: 21 December 2023
© Author(s) 2023. CC BY 4.0 License.

However, this is not a consistent observation across all salinity zones. We found that there is a significant negative relationship ($p < 0.05$) between the concentrations of NO and DIN, NO_3^-, NO_2^-, NH_4^+, sum of NO_2^- and NH_4^+, and N_2O in the limnic zone, and between NO and NO_2^- in the coastal-brackish zone; whereas there is a significant positive correlation ($p < 0.05$) between concentrations of NO and NO_2^-, N_2O, and sum of NO_2^- and NH_4^+ in the Hamburg Port area. In the next section, we will try to explain the different processes that contributed to this trend.

4.4 Biological production of NO

NO can be produced or consumed by bacteria and phytoplankton. We explored the possibility of NO production from phytoplankton (e.g., Wang et al., 2020; Kim et al., 2006) as NO may be generally consumed or produced by phytoplankton while they bloom and/or in response to environmental stress and pollution (Estevez and Puntarulo, 2005; Mallick et al., 2002; Zhang et al., 2006). However, we noted that chlorophyll a concentrations were minimal (< 6.50 µg L^{-1}) at areas where the NO concentration peaked (i.e., Elbe 623.40 and 628.04), suggesting that phytoplankton bloom may not be a major factor contributing to higher dissolved NO concentration in our study site. Similar to the findings of Tian et al. (2021), the NO distribution in the Elbe Estuary is not related to the distribution of chlorophyll a ($p > 0.05$, Table S3).

As discussed earlier, Ayeni et al. (2021) suggested that nitrogen cycling processes (nitrification, denitrification, and anammox) may have influenced NO distribution in river systems. In this study, anammox was ruled out as a source of NO in the water column due to the oxygen concentrations of >130 µM, indicative of oxic conditions (Okabe et al., 2023; Kalvelage et al., 2011) that are known to inhibit anammox.

Now, we investigate two other nitrogen cycling processes that could produce NO in the Elbe Estuary – nitrification (see Kozlowski et al., 2016; Caranto and Lancaster, 2017; and Ward and Zafiriou, 1988) and nitrifier-denitrification (see Wrage et al., 2001; Nils, 2003; Zumft, 1997; and Koops and Pommerening-Röser, 2001).

4.4.1 Nitrification in the Elbe Estuary

Recently, Gong et al. (2023) noted nitrification as the major contributor to microbial production of NO in the coastal seas of the Yellow and East China Seas. Prior studies suggest nitrification as the main production pathway of N_2O in the Elbe Estuary (Brase et al., 2017; Schulz et al., 2023). In this study, we noted that nitrification occurs in the entire stretch of the study site based on the plots of AOU and excess N_2O (Fig. 7a), as AOU correlates significantly with the ΔN_2O in all three salinity zones. In the coastal-brackish and limnic zones, we observed a significant positive linear relationship (Table 1, see also Fig. S7h-j) between NO and the ratio of N_2O and precursor substrates of nitrification, NH_4^+, and NO_2^-, and the sum of NH_4^+ and NO_2^-. Additionally, in these two salinity zones, a significant positive linear relationship exists between N_2O and NO_3^- (Fig. S5b), the final product of nitrification. These findings point to NO production via nitrification.

As mentioned in Sect. 3.2, significant inverse relationships were also observed between NO and the nitrogen-containing nutrients (Table 1, see Fig. S7a-e) alongside N_2O (Fig. S7g) in the limnic zone. We also observed a significant inverse relationship between NO vs. NO_2^- (Table 1, Fig. S7c) and NO vs NO_2^-/O_2 ratio (Fig. S7f) in both the coastal-brackish and

https://doi.org/10.5194/egusphere-2023-3009
Preprint. Discussion started: 21 December 2023
© Author(s) 2023. CC BY 4.0 License.

limnic zones. We speculate that the observed trends in the coastal-brackish and coastal zones could be partly attributed to NH_4^+ limitation (see Fig. 3) and the well-oxygenated water surface. NH_4^+, upon nitrification in a well-oxygenated water column, is being consumed in the process, increasing the NO concentration and resulting in the observed inverse correlation. During the nitrification process, NO is subsequently consumed as it undergoes further oxidation to NO_2^- and eventually to NO_3^-. Furthermore, we observed that five sampling sites in the coastal-brackish zone with $O_2 > 200$ µM had NO concentrations less than the detection limit (Fig. 6).

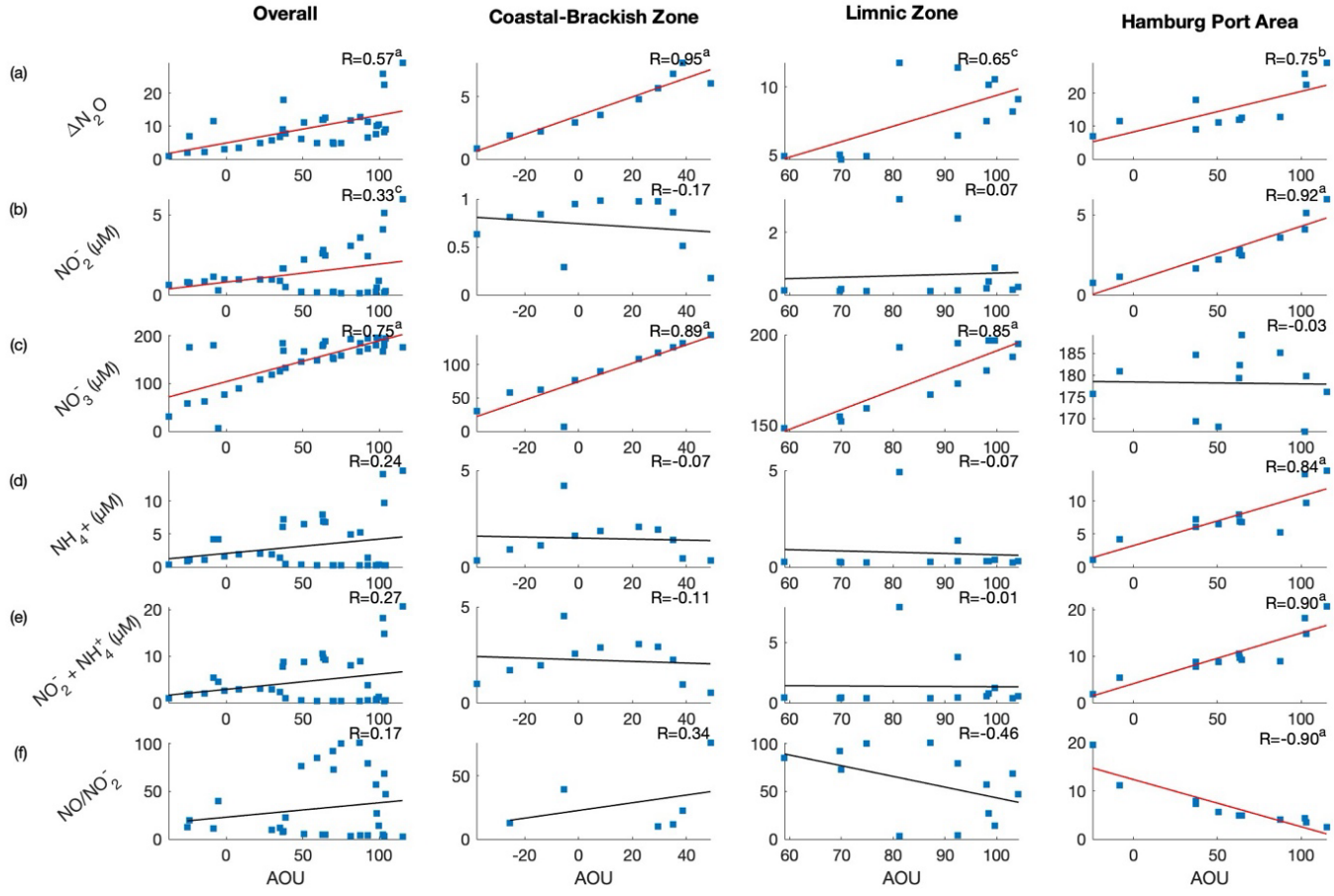

Figure 7: Scatter plots between AOU and ΔN_2O, NO_2^- (µM), NO_3^-(µM), NH_4^+(µM), sum of NO_2^- + NH_4^+ (µM), and NO/NO_2^- ratio. Note that the superscripts on the R-value indicate a significant correlation at [a] $p < 0.001$, [b] $p < 0.01$, and [c] $p < 0.05$. Significant correlations are denoted with a red regression line. We observed significant correlations between AOU and NO_3^- in the coastal-brackish and limnic zones, indicating nitrification as a dominant process. Meanwhile, we noted a significant correlation between AOU and NO_2^- and NO/ NO_2^- ratio, potentially indicating denitrification/nitrifier-denitrification process.

https://doi.org/10.5194/egusphere-2023-3009
Preprint. Discussion started: 21 December 2023
© Author(s) 2023. CC BY 4.0 License.

4.4.2 Nitrifier-denitrification/denitrification in the Hamburg Port area

In contrast to the brackish-coastal and limnic zones, where NH_4^+ and NO_2^- concentrations are relatively minimal (see Sect. 4.2), we noted elevated concentrations of NH_4^+ and NO_2^- (>1 µM) in the Hamburg Port area. Because NH_4^+ and NO_2^- are not limited in this section of the Elbe Estuary, when the nitrification reaction proceeds, direct linear relationships between the concentrations of NO and NO_2^- and the sum of NH_4^+ and NO_2^- were observed (Table 1, see also Fig. S7c and Fig. S7e).

In addition to nitrification, we therefore hypothesize the concurrent presence of nitrifier-denitrification and/or denitrification processes in the Hamburg Port area during our sampling period. Unlike the brackish-coastal and limnic zones, we did not observe a significant linear relationship between AOU and NO_3^- (Fig. 7c) in the Hamburg Port area. Instead, we found significant linear relationships ($p<0.001$) between AOU and NO_2^- (Fig. 7b), NH_4^+ (Fig. 7d), and the sum of NO_2^- and NH_4^+ (Fig. 7e).

Furthermore, significant negative correlation ($p < 0.0001$) with O_2 and NO_2^-, NH_4^+, and N_2O were observed (Fig. S6). Moreover, distinct peaks of NO_2^- (> 4 µM) and NH_4^+ (> 9.5 µM) were measured at the sampling sites in the Hamburg Port area at Elbe-km 628.04, 628.21, and 623.40, with the lowest O_2 concentrations (<150 µM) in this campaign (Fig. 3). In this sampling locations, relatively higher concentrations of NO (> 14 pM) and N_2O (> 30 µM) were also measured. At these sampling stations, the N_2O and NO saturations were exceedingly high, reaching values over 360% and 270%, respectively. These high NO and N_2O saturations are notable, as they suggest a significant level of production.

While there is a significant linear relationship between NO and N_2O (Fig. 7g) in the Hamburg Port area, there is no linear correlation between NO_3^- vs. NO (Fig. S7b) and N_2O (Fig. S5b), likely attributed to NO_3^- consumption processes in this area, a finding supported by the observed minimal decrease in NO_3^- concentrations (Fig. 3). The observed decrease in NO_3^- coupled with an increase in N_2O and NO concentrations further suggests the potential occurrence of denitrification or nitrifier-denitrification processes.

The measured O_2 concentrations in the Hamburg Port area could inhibit denitrification. Nevertheless, oxygen-limited conditions often found in sediments and within biofilms on suspended particles (see e.g., Xia et al., 2017) in estuaries provide suitable microenvironments for nitrifying bacteria to switch from nitrification to nitrifier-denitrification (see Schulz et al., 2022; Dai et al., 2008). Previous research (Schroeder, 1997; Sanders et al., 2018; van Beusekom et al., 2021; Brase et al., 2017) indicated that low oxygen conditions may develop in the Hamburg Port area due to its geomorphological features and high nutrient content, particularly from runoff and remineralization process. Brase et al. (2017) reported that the Hamburg Port area is a hotspot for N_2O production attributed to both nitrification and nitrifier-denitrification processes. Prior studies confirmed the highest denitrification rates in the sediments (Deek et al., 2013) and the highest nitrification rates in the water column at this section of the Elbe Estuary (Sanders et al., 2018).

https://doi.org/10.5194/egusphere-2023-3009
Preprint. Discussion started: 21 December 2023
© Author(s) 2023. CC BY 4.0 License.

5. Conclusion

Our study provides the first measurement of dissolved NO in the Elbe Estuary, shedding light on the potential sources and processes driving NO production in this area. We observed variations in NO concentrations and flux densities along the salinity gradient, with elevated levels in the Hamburg Port area. During this campaign, the lower Elbe Estuary and Hamburg Port area were a source of NO to the atmosphere with a mean (± SD) of 2.40 (±1.54) × 10^{-17} mol cm^{-2} s^{-1}. Notably, the Hamburg Port area showed a higher mean flux density of 3.47 (±1.43) × 10^{-17} mol cm^{-2} s^{-1}.

Furthermore, areas with higher NO_2^- and NH_4^+ concentrations, which primarily come from anthropogenic sources like wastewater discharge, agricultural runoff, and industrial effluents, exhibited elevated dissolved NO concentrations. This finding emphasizes the importance of NO_2^- as a potential source of NO during NO_2^- photolysis or NH_4^+–related transformation processes such as nitrification or nitrifier/denitrification.

Eutrophication, characterized by excessive nutrient inputs and algal blooms, could substantially impact NO concentrations in estuaries. During eutrophication, increased nutrient availability stimulates algal growth, leading to oxygen depletion at night or daybreak, as algae consume oxygen through respiration. As the algal blooms eventually die off and decompose, microbial processes like nitrification and denitrification thrive under low oxygen conditions, potentially releasing NO and N_2O.

Further investigation is necessary to elucidate the potential seasonal variability in NO concentrations within the Elbe Estuary. Seasonal fluctuations significantly influence NO_2^- and NH_4^+ loading (Malinowski et al., 2020), particularly during the spring and summer when agricultural practices intensify and nitrogen-based fertilizers are used extensively (Pastuszak et al., 2018). These factors contribute to increased NO_2^- and NH_4^+ concentrations in the estuary, primarily due to heightened surface runoff and leaching from agricultural areas. Additionally, in the Hamburg Port area, the decomposition of phytoplankton from the Elbe River may contribute to increased NO_2^- and NH_4^+ concentrations due to remineralization. This could subsequently lead to oxygen depletion, especially during the warmer summer months, coinciding with increased microbial activity that could intensify nitrogen transformation processes (Schulz et al., 2023; Sanders et al., 2018). No comprehensive study to date has examined the seasonal dynamics of NO concentrations in such contexts.

Moreover, despite nitrogen-containing nutrient concentrations in the Elbe Estuary being higher than those reported in previous studies in other regions, the NO concentrations remained low. This observation prompts further investigation into how nitrogen transformation processes could influence NO distribution in the Elbe Estuary. It is recommended that future research adopt a more comprehensive approach, incorporating both higher temporal resolution and spatially diverse sampling strategies. This combined approach will enable a more nuanced understanding of the dynamic interplay between various controlling factors influencing NO concentration in the coastal and estuarine environments.

Acknowledgment

We would like to thank the captain and crew of the R/V Ludwig Prandtl for their assistance and support during the fieldwork. Likewise, we would also like to express our gratitude to our colleagues from the Helmholtz-Zentrum Hereon, who participated

© Author(s) 2023. CC BY 4.0 License.

in the sampling and invited our research group to join this field campaign. We would also like to thank Dr. Annette Kock, who assisted in the logistics of this field campaign, and Ms. Estela Monteiro for providing helpful comments on the earlier version of the manuscript. Riel Carlo O. Ingeniero is supported by DAAD Research Grants – Doctoral Programmes in Germany (57440921).

Data Availability Statement

The data sets generated and/or analyzed in this study can be accessed by contacting the corresponding author and will be made publicly available at coastMap Geoportal (www.coastmap.org), which connects to PANGAEA, with future DOI availability anticipated.

Authors Contribution

RI conceptualized and designed the study, carried out field sampling and analysis, and authored the manuscript. GS managed the research cruise, performed laboratory analyses of supplementary biogeochemical parameters, and contributed a critical review of the manuscript. HB assisted with study conceptualization, supervision, and a critical review of the manuscript.

Competing Interest

At least one of the (co-)authors is a member of the editorial board of Biogeosciences.

References

Abada, A., Beiralas, R., Narvaez, D., et al.: Aerobic bacteria produce nitric oxide via denitrification and promote algal population collapse, ISME J, 17, 1167–1183, https://doi.org/10.1038/s41396-023-01427-8, 2023.

Adesina, A. O. and Sakugawa, H.: Photochemically generated nitric oxide in seawater: The peroxynitrite sink and its implications for daytime air quality, Sci Total Environ, 781, 146683, https://doi.org/10.1016/j.scitotenv.2021.146683, 2021.

Adesina, A. O., Anifowose, A. J., Takeda, K., and Sakugawa, H.: Photogeneration and interactive reactions of three reactive species in the Seto Inland Sea, Japan, Environ Chem, 15, 236, https://doi.org/10.1071/en18035, 2018.

Amann, T., Weiss, A., and Hartmann, J.: Carbon dynamics in the freshwater part of the Elbe estuary, Germany: Implications of improving water quality, Estuar Coast Shelf Sci, 107, 112–121, https://doi.org/10.1016/j.ecss.2012.05.012, 2012.

Anifowose, A. and Sakugawa, H.: Determination of daytime flux of nitric oxide radical (NO•) at an inland sea–atmospheric boundary in Japan, Journal of Aquatic Pollution and Toxicology, 1, 10, 2017.

Anifowose, A. J., Takeda, K., and Sakugawa, H.: Photoformation rate, steady-state concentration and lifetime of nitric oxide radical (NO) in a eutrophic river in Higashi-Hiroshima, Japan, Chemosphere, 119, 302–309, https://doi.org/10.1016/j.chemosphere.2014.06.063, 2015.

© Author(s) 2023. CC BY 4.0 License.

Ayeni, T. T., Jadoon, W. A., Adesina, A. O., Sunday, M. O., Anifowose, A. J., Takeda, K., and Sakugawa, H.: Measurements, sources and sinks of photoformed reactive oxygen species in Japanese rivers, Geochem J, 55, 89–102, https://doi.org/10.2343/geochemj.2.0620, 2021.

Birks, J. W., Turnipseed, A. A., Andersen, P. C., Williford, C. J., Strunk, S., Carpenter, B., and Ennis, C. A.: Portable calibrator for NO based on the photolysis of N_2O and a combined NO_2/NO/O_3 source for field calibrations of air pollution monitors, Atmos Meas Tech, 13, 1001–1018, https://doi.org/10.5194/amt-13-1001-2020, 2020.

Borges, A., Vanderborght, J.-P., Schiettecatte, L.-S., Gazeau, F., Ferrón-Smith, S., Delille, B., and Frankignoulle, M.: Variability of gas transfer velocity of CO_2 in a macrotidal estuary (The Scheldt), Estuaries, 27, 593–603, https://doi.org/10.1007/BF02907647, 2004.

Brase, L., Bange, H. W., Lendt, R., Sanders, T., and Dähnke, K.: High Resolution Measurements of Nitrous Oxide (N2O) in the Elbe Estuary, Frontiers Mar Sci, 4, 162, https://doi.org/10.3389/fmars.2017.00162, 2017.

Burchard, H., Schuttelaars, H. M., and Ralston, D. K.: Sediment Trapping in Estuaries., Annu Rev Mar Sci, 10, 371–395, https://doi.org/10.1146/annurev-marine-010816-060535, 2017.

Caranto, J. D., and Lancaster, K. M.: Nitric oxide is an obligate bacterial nitrification intermediate produced by hydroxylamine oxidoreductase. Proc. Natl. Acad. Sci. U.S.A., 114(30), 5573–5581. https://doi.org/10.1073/pnas.1704504114m, 2017.

Dähnke, K., Bahlmann, E., and Emeis, K.: A nitrate sink in estuaries? An assessment by means of stable nitrate isotopes in the Elbe estuary, Limnol Oceanogr, 53, 1504–1511, https://doi.org/10.4319/lo.2008.53.4.1504, 2008.

Dähnke, K., Sanders, T., Voynova, Y., and Wankel, S. D.: Nitrogen isotopes reveal a particulate-matter-driven biogeochemical reactor in a temperate estuary, Biogeosciences, 19, 5879–5891, https://doi.org/10.5194/bg-19-5879-2022, 2022.

Dai, M., Wang, L. F., Guo, X., Zhai, W., Li, Q. X., He, B., and Kao, S. J.: Nitrification and inorganic nitrogen distribution in a large perturbed river/estuarine system: the Pearl River Estuary, China. Biogeosciences, 5, 1227-1244. https://doi.org/10.5194/bg-5-1227-2008, 2008.

Deek, A., Dähnke, K., Beusekom, J. van, Meyer, S., Voss, M., and Emeis, K.: N_2 fluxes in sediments of the Elbe Estuary and adjacent coastal zones, Mar Ecol Prog Ser, 493, 9–21, https://doi.org/10.3354/meps10514, 2013.

Estevez, M. S. and Puntarulo, S.: Nitric oxide generation upon growth of Antarctic Chlorella sp. cells, Physiol Plantarum, 125, 192–201, https://doi.org/10.1111/j.1399-3054.2005.00561.x, 2005.

Fanning, K. A.: Influence of atmospheric pollution on nutrient limitation in the ocean, Nature, 339, 460–463, https://doi.org/10.1038/339460a0, 1989.

Geerts, L., K. Wolfstein, S. Jacobs, S. van Damme, and W. Vandenbruwaene. 2012. Zonation of the TIDE estuaries. Tide Report. http://www.tide-toolbox.eu/pdf/reports/Zonation_of_the_TIDE_estuaries

Gill, A. (1983). Atmosphere-Ocean Dynamics (Vol. 30). Academic Press.

Gong, J.-C., Jin, H., Li, B.-H., Tian, Y., Liu, C.-Y., Li, P.-F., Liu, Q., Ingeniero, R. C. O., and Yang, G.-P.: Emissions of Nitric Oxide from Photochemical and Microbial Processes in Coastal Waters of the Yellow and East China Seas, Environ Sci Technol, 57, 4039–4049, https://doi.org/10.1021/acs.est.2c08978, 2023.

https://doi.org/10.5194/egusphere-2023-3009
Preprint. Discussion started: 21 December 2023
© Author(s) 2023. CC BY 4.0 License.

Haagen-Smit, A. J. and Fox, M. M.: Photochemical Ozone Formation with Hydrocarbons and Automobile Exhaust, Air Repair, 4, 105–136, https://doi.org/10.1080/00966665.1954.10467649, 1954.

Hamburger Luftmessnetz: https://luft.hamburg.de/, last accessed: 2 May 2023.

Hein, H., Hein, B., Mai, S., and Barjenbruch, U.: The Residence Time in the Elbe River Focusing on the Estuary, in: ICHE 2014. Proceedings of the 11th International Conference on Hydroscience & Engineering, edited by Lehfeldt, R. and Kopmann, R., Bundesanstalt für Wasserbau, Karlsruhe, 837–844, 2014.

Hein, S. S. V., Sohrt, V., Nehlsen, E., Strotmann, T., and Fröhle, P.: Tidal Oscillation and Resonance in Semi-Closed Estuaries—Empirical Analyses from the Elbe Estuary, North Sea, Water-sui, 13, 848, https://doi.org/10.3390/w13060848, 2021.

IPCC: Climate Change 2021: The Physical Science Basis. Contribution of Working Group I to the Sixth Assessment Report of the Intergovernmental Panel on Climate Change, Cambridge University Press, Cambridge, United Kingdom and New York, NY, USA, https://doi.org/10.1017/9781009157896, 2021.

Jaeglé, L., Steinberger, L., Martin, R. V., and Chance, K.: Global partitioning of NO x sources using satellite observations: Relative roles of fossil fuel combustion, biomass burning and soil emissions, Faraday Discuss, 130, 407–423, https://doi.org/10.1039/b502128f, 2005.

Jeffrey, S. W. and Humphrey, G. F.: New spectrophotometric equations for determining chlorophylls a, b, c1, and c2 in higher plants, algae, and natural phytoplankton, Biochem. Physiol. Pflanzen, 167, 191-197, https://doi.org/10.1016/S0015-3796(17)30778-3,1975

Kalvelage, T., Jensen, M. M., Contreras, S., Revsbech, N. P., Lam, P., Günter, M., LaRoche, J., Lavik, G., and Kuypers, M. M. M.: Oxygen Sensitivity of Anammox and Coupled N-Cycle Processes in Oxygen Minimum Zones, PLoS ONE, 6, e29299, https://doi.org/10.1371/journal.pone.0029299, 2011.

Kappenberg, J. and Grabemann, I.: Variability of the mixing zones and estuarine turbidity maxima in the Elbe and Weser estuaries, Estuaries, 24, 699–706, https://doi.org/10.2307/1352878, 2001.

Kerner, M.: Effects of deepening the Elbe Estuary on sediment regime and water quality, Estuar Coast Shelf Sci, 75, 492–500, https://doi.org/10.1016/j.ecss.2007.05.033, 2007.

Kim, D., Yamaguchi, K., and Oda, T.: Nitric oxide synthase-like enzyme mediated nitric oxide generation by harmful red tide phytoplankton, Chattonella marina, J Plankton Res, 28, 613–620, https://doi.org/10.1093/plankt/fbi145, 2006.

Koops, H. and Pommerening-Röser, A.: Distribution and ecophysiology of the nitrifying bacteria emphasizing cultured species, Fems Microbiol Ecol, 37, 1–9, https://doi.org/10.1111/j.1574-6941.2001.tb00847.x, 2001.

Kozlowski, J. A., Stieglmeier, M., Schleper, C., Klotz, M. G., and Stein, L. Y.: Pathways and key intermediates required for obligate aerobic ammonia-dependent chemolithotrophy in bacteria and Thaumarchaeota. The ISME Journal, 10, 1836–1845, https://doi.org/ 10.1038/ismej.2016.2, 2016.

Kuypers, M. M. M., Marchant, H. K., and Kartal, B.: The microbial nitrogen-cycling network, Nat Rev Microbiol, 16, 263–276, https://doi.org/10.1038/nrmicro.2018.9, 2018.

https://doi.org/10.5194/egusphere-2023-3009
Preprint. Discussion started: 21 December 2023
© Author(s) 2023. CC BY 4.0 License.

Lancaster, J. R.: A Tutorial on the Diffusibility and Reactivity of Free Nitric Oxide, Nato Sci S A Lif Sci, 1, 18–30, https://doi.org/10.1006/niox.1996.0112, 1997.

Lewis, R. S. and Deen, W. M.: Kinetics of the Reaction of Nitric Oxide with Oxygen in Aqueous Solutions, Chem Res Toxicol, 7, 568–574, https://doi.org/10.1021/tx00040a013, 1994.

Likens, G. E., Wright, R. F., Galloway, J. N., and Butler, T. J.: Acid Rain, Sci Am, 241, 43–51, https://doi.org/10.1038/scientificamerican1079-43, 1979.

Liu, C.-Y., Feng, W.-H., Tian, Y., Yang, G.-P., Li, P.-F., and Bange, H. W.: Determination of dissolved nitric oxide in coastal waters of the Yellow Sea off Qingdao, Ocean Sci., 13, 623–632, https://doi.org/10.5194/os-13-623-2017, 2017.

Lutterbeck, H. E. and Bange, H. W.: An improved method for the determination of dissolved nitric oxide (NO) in seawater samples, Ocean Sci, 11, 937–946, https://doi.org/10.5194/os-11-937-2015, 2015.

Lutterbeck, H. E., Arévalo-Martínez, D. L., Löscher, C. R., and Bange, H. W.: Nitric oxide (NO) in the oxygen minimum zone off Peru, Deep Sea Res Part Ii Top Stud Oceanogr, 156, 148–154, https://doi.org/10.1016/j.dsr2.2017.12.023, 2018.

Malinowski, M., Alawi, M., Krohn, I., Ruff, S., Indenbirken, D., Alawi, M., Karrasch, M., Lüschow, R., Streit, W. R., Timmermann, G., and Pommerening-Röser, A.: Deep amoA amplicon sequencing reveals community partitioning within ammonia-oxidizing bacteria in the environmentally dynamic estuary of the River Elbe, Sci Rep-uk, 10, 17165, https://doi.org/10.1038/s41598-020-74163-0, 2020.

Mallick, N., Mohn, F. H., Soeder, C. J., and Grobbelaar, J. U.: Ameliorative role of nitric oxide on H2O2 toxicity to a chlorophycean alga Scenedesmus obliquus, J Gen Appl Microbiol, 48, 1–7, https://doi.org/10.2323/jgam.48.1, 2002.

Nils, R.-P.: Coupled nitrification-denitrification in autotrophic and heterotrophic estuarine sediments: On the influence of benthic microalgae, Limnol Oceanogr, 48, 93–105, https://doi.org/10.4319/lo.2003.48.1.0093, 2003.

Norbisrath, M., Pätsch, J., Dähnke, K., Sanders, T., Schulz, G., Beusekom, J. E. E. van, and Thomas, H.: Metabolic alkalinity release from large port facilities (Hamburg, Germany) and impact on coastal carbon storage, Biogeosciences, 19, 5151–5165, https://doi.org/10.5194/bg-19-5151-2022, 2022.

Okabe, S., Ye, S., Lan, X., Nukada, K., Zhang, H., Kobayashi, K., and Oshiki, M.: Oxygen tolerance and detoxification mechanisms of highly enriched planktonic anaerobic ammonium-oxidizing (anammox) bacteria, ISME Commun., 3, 45, https://doi.org/10.1038/s43705-023-00251-7, 2023.

Olasehinde, E. F., Takeda, K., and Sakugawa, H.: Photochemical Production and Consumption Mechanisms of Nitric Oxide in Seawater, Environ Sci Technol, 44, 8403–8408, https://doi.org/10.1021/es101426x, 2010.

Pastuszak, M., Kowalkowski, T., Kopiński, J., Doroszewski, A., Jurga, B., and Buszewski, B.: Long-term changes in nitrogen and phosphorus emission into the Vistula and Oder catchments (Poland)—modeling (MONERIS) studies, Environ Sci Pollut R, 25, 29734–29751, https://doi.org/10.1007/s11356-018-2945-7, 2018.

Pastuszak, M., Kowalkowski, T., Kopiński, J., Doroszewski, A., Jurga, B., and Buszewski, B.: Long-term changes in nitrogen and phosphorus emission into the Vistula and Oder catchments (Poland)—modeling (MONERIS) studies, Environ Sci Pollut R, 25, 29734–29751, https://doi.org/10.1007/s11356-018-2945-7, 2018.

https://doi.org/10.5194/egusphere-2023-3009
Preprint. Discussion started: 21 December 2023
© Author(s) 2023. CC BY 4.0 License.

Petersen, W.: FerryBox systems: State-of-the-art in Europe and future development, J. Mar. Syst., 140, 4–12, https://doi.org/10.1016/j.jmarsys.2014.07.003, 2014

Ruiz-Martinez, G.: 2021. Seawater density from salinity, temperature and pressure. MATLAB Central File Exchange. Available at: https://www.mathworks.com/matlabcentral/fileexchange/85900-seawater-density-from-salinity-temperature-and-pressure, last access: 5 June 2023.

Sanders, T., Schöl, A., and Dähnke, K.: Hot Spots of Nitrification in the Elbe Estuary and Their Impact on Nitrate Regeneration, Estuaries Coasts, 41, 128–138, https://doi.org/10.1007/s12237-017-0264-8, 2018.

Schreiber, F., Wunderlin, P., Udert, K. M., and Wells, G. F.: Nitric oxide and nitrous oxide turnover in natural and engineered microbial communities: biological pathways, chemical reactions, and novel technologies, Front Microbiol, 3, 372, https://doi.org/10.3389/fmicb.2012.00372, 2012.

Schroeder, F.: Water quality in the Elbe estuary: Significance of different processes for the oxygen deficit at Hamburg, Environ Model Assess, 2, 73–82, https://doi.org/10.1023/a:1019032504922, 1997.

Schulz, G., Sanders, T., Beusekom, J. E. E. van, Voynova, Y. G., Schöl, A., and Dähnke, K.: Suspended particulate matter drives the spatial segregation of nitrogen turnover along the hyper-turbid Ems estuary, Biogeosciences, 19, 2007–2024, https://doi.org/10.5194/bg-19-2007-2022, 2022.

Schulz, G., Sanders, T., Voynova, Y. G., Bange, H. W., and Dähnke, K.: Seasonal variability of nitrous oxide concentrations and emissions in a temperate estuary, Biogeosciences, 20, 3229–3247, https://doi.org/10.5194/bg-20-3229-2023, 2023.

Sharqawy, M. H., V, J. H. L., and Zubair, S. M.: Thermophysical properties of seawater: a review of existing correlations and data, Desalin Water Treat, 16, 354–380, https://doi.org/10.5004/dwt.2010.1079, 2012.

Tian, Y., Wang, K.-K., Yang, G.-P., Li, P.-F., Liu, C.-Y., Ingeniero, R. C. O., and Bange, H. W.: Continuous Chemiluminescence Measurements of Dissolved Nitric Oxide (NO) and Nitrogen Dioxide (NO2) in the Ocean Surface Layer of the East China Sea, Environ Sci Technol, https://doi.org/10.1021/acs.est.0c06799, 2021.

Tian, Y., Xue, C., Liu, C.-Y., Yang, G.-P., Li, P.-F., Feng, W.-H., and Bange, H. W.: Nitric oxide (NO) in the Bohai Sea and the Yellow Sea, Biogeosciences, 16, 4485–4496, https://doi.org/10.5194/bg-16-4485-2019, 2019.

Tian, Y., Yang, G.-P., Liu, C.-Y., Li, P.-F., Chen, H.-T., and Bange, H. W.: Photoproduction of nitric oxide in seawater, Ocean Sci, 16, 135–148, https://doi.org/10.5194/os-16-135-2020, 2020.

Treinin, A. and Hayon, E.: Absorption spectra and reaction kinetics of NO2, N2O3, and N2O4 in aqueous solution, J Am Chem Soc, 92, 5821–5828, https://doi.org/10.1021/ja00723a001, 1970.

van Beusekom, J. E. E. van, Fehling, D., Bold, S., and Sanders, T.: Pelagic oxygen consumption rates in the Elbe estuary: Proxies and spatial patterns., https://doi.org/10.5194/egusphere-egu21-8699, 2021.

Wang, K. K., Tian, Y., Li, P. F., Liu, C. Y., & Yang, G. P. Sources of nitric oxide during the outbreak of Ulva prolifera in coastal waters of the Yellow Sea off Qingdao. Marine Environmental Research, 162, 105177, https://doi.org/10.1016/j.marenvres.2020.105177, 2020.

https://doi.org/10.5194/egusphere-2023-3009
Preprint. Discussion started: 21 December 2023
© Author(s) 2023. CC BY 4.0 License.

Ward, B. B. and Zafiriou, O. C.: Nitrification and nitric oxide in the oxygen minimum of the eastern tropical North Pacific, Deep Sea Res Part Oceanogr Res Pap, 35, 1127–1142, https://doi.org/10.1016/0198-0149(88)90005-2, 1988.

Wise, D. L., and Houghton, G.: Diffusion coefficients of neon, krypton, xenon, carbon monoxide and nitric oxide in water at 10–60°C, Chem. Eng. Sci., 23, 1211–1216, doi.org:10.1016/0009-2509(68)89029-3, 1968

Wrage, N., Velthof, G. L., Beusichem, M. L. van, and Oenema, O.: Role of nitrifier denitrification in the production of nitrous oxide, Soil Biology Biochem, 33, 1723–1732, https://doi.org/10.1016/s0038-0717(01)00096-7, 2001.

Xia, X., Liu, T., Yang, Z., Michalski, G., Liu, S., Jia, Z., & Zhang, S. (2017). Enhanced nitrogen loss from rivers through coupled nitrification-denitrification caused by suspended sediment. Science of The Total Environment, 579, 602-612. https://doi.org/10.1016/j.scitotenv.2016.10.181, 2017.

Zacharia, I. G. and Deen, W. M.: Diffusivity and Solubility of Nitric Oxide in Water and Saline, Ann Biomed Eng, 33(2), 214-222, https://doi.org/10.1007/s10439-005-8980-9, 2005.

Zafiriou, O. C. and McFarland, M.: Nitric oxide from nitrite photolysis in the central equatorial Pacific, J Geophys Res, 86, 3173, https://doi.org/10.1029/jc086ic04p03173, 1981.

Zafiriou, O. C., McFarland, M., and Bromund, R. H.: Nitric Oxide in Seawater, Science, 207, 637–639, https://doi.org/10.1126/science.207.4431.637, 1980.

Zhang, Z.-B., Liu, C.-Y., Wu, Z.-Z., Xing, L., and Li, P.-F.: Detection of nitric oxide in culture media and studies on nitric oxide formation by marine microalgae., Medical Sci Monit Int Medical J Exp Clin Res, 12, BR75-85, 2006.

Zumft, W. G.: Cell biology and molecular basis of denitrification., Microbiol Mol Biology Rev Mmbr, 61, 533–616, https://doi.org/10.1128/mmbr.61.4.533-616.1997,1997.